Slow and fast light in three-beam interferometers: Theory and experiment

J. Arias,[1] A. Sánchez-Meroño,[1] M. M. Sánchez-López,[2] and I. Moreno[1]

[1]*Departamento de Ciencia de Materiales, Óptica y Tecnología Electrónica, Universidad Miguel Hernández, 03202 Elche, Spain*

[2]*Instituto de Bioingeniería, Universidad Miguel Hernández, 03202 Elche, Spain*

(Received 8 November 2011; revised manuscript received 2 February 2012; published 16 March 2012)

We demonstrate the generation of slow and fast light (SFL) in a linear and passive three-beam interferometer. Such propagation regimes occur for narrowband pulses with center frequency close to the transmission minima. A model that fully describes SFL effects in this system is developed and an analytical approximate expression for the group delay at the minima is derived. We demonstrate that slow light is not possible if the length difference between adjacent branches of the interferometer is a constant. If a small length detuning (ξ) in one of the branches is introduced, slow light at one of the two minima can be obtained as long as ξ exceeds a critical value. Simultaneously, tunneling, superluminal, or normal regime is sustained at the other minimum, depending on the system's length. A proof-of-model experiment is performed in the radiofrequency range using coaxial cables and 1×3 power splitters. The possible realization and performance of such a system in the optical range is also discussed. This system is proposed as a simple alternative to active systems and photonic band-gap structures for sustaining both slow and fast light.

DOI: 10.1103/PhysRevA.85.033815 PACS number(s): 42.25.Bs, 42.25.Hz, 73.40.Gk

I. INTRODUCTION

Research on slow and fast light (SFL) systems has increased in recent years in the photonics community. Although the possibility of propagating a light pulse in dispersive media at unusually slow or fast group velocity is been known for many decades [1], interest in this phenomena has been triggered by their promising applications in optical communications systems. In particular, the use of optical instead of electronic delay lines and the development of optical buffers, switches and synchronizers based on SFL systems have been suggested [2–4].

The group velocity of a pulse is the velocity at which the peak of its envelope propagates and is related to the frequency (ω) variation of the medium's refractive index n by

$$v_g = \frac{c}{n + \omega \frac{dn}{d\omega}}. \tag{1}$$

Thus, a steep positive spectral variation of the refractive index ($dn/d\omega > 0$) can lead to a very small group velocity ($v_g \ll c$) (*slow light* or subluminal pulse propagation), whereas in the case of steep anomalous dispersion ($dn/d\omega < 0$) the group velocity can be larger than the speed of light in vacuum c (superluminal pulse propagation) or even negative (pulse tunneling). These latter cases are known as *fast light*. Because of the Kramers-Kronig relations, such abnormal pulse propagation regimes are associated to sharp spectral features in the transmission spectrum [5].

Experimental evidence of SFL has been reported for a myriad of systems exhibiting material resonances (gain or absorption), like Bose-Einstein condensates [6], atomic vapors [7], solid crystals [8,9], semiconductor waveguides [10], semiconductor quantum wells and dots [11], and in optical fibers [12–14]. It has also been reported in systems exhibiting structural resonances (photonic band-gap systems, PBG), like photonic crystals [15] and fiber Bragg gratings [16,17], where the dispersion is due to coupling between the incident wavelength and the system's characteristic length. For such PBG systems, experimental evidence of SFL has also been provided in the microwave [18–20] and radio-frequency (RF) [21,22] range. In fact, lower frequency setups have been relevant to clarify important issues, like the puzzling advancement of the outgoing pulse peak with respect to the incident pulse in tunneling experiments (negative v_g) [23], and have provided experimental evidence of a theoretically proposed structure exhibiting negative group delays in reflection [20]. They have been also used to explore quasiperiodic structures, such as Fibonacci or Thue-Morse, exhibiting strong normal and anomalous dispersion [24].

Regardless of the frequency range, let us note that all the aforementioned systems are either active (they respond to the interaction with light by generating narrow, gain, or absorption spectral bands) [6–11], exhibit nonlinear effects [12–14], or are periodically structured [15–22,24]. Unlike them, we have investigated the occurring of SFL effects in passive, linear, and nonperiodical structures. In a previous work [25], we demonstrated superluminal and negative group velocity in a linear and passive Mach-Zehnder interferometer (MZI) operative in the RF range. This behavior had also been outlined in Ref. [26] for an equivalent system consisting of a single asymmetric loop structure. We noted that anomalous dispersion in a narrow frequency region around the interferometer's transmission minima is strong enough to hold fast light without the need of microstructuring, doping, or using nonlinear media in the interferometer's arms. Slow light was, however, not observed in a MZI [25]. Slow light is particularly interesting since it improves the spectral sensitivity of interferometers [27] and enhances light-matter interaction and hence nonlinear effects [3].

Interestingly, the series loop structures studied by El Boudouti *et al.* [26] do present subluminal regime when defects are introduced. These structures may be regarded as MZIs (asymmetric loops) connected in series through segments. Like PBG systems, they exhibit bandgaps, and defect modes appear inside the transmission gaps if one of the segments connecting the loops is somehow changed (in length, for example). The

situation resembles that of a doped photonic crystal, with superluminal propagation for a pulse with center frequency in the bandgap and subluminal propagation for a pulse with center frequency at the defect mode. But unlike photonic crystals, an outstanding characteristic of this serial loop structure is the existence of bandgaps in a totally homogeneous material, without the need of refractive index contrast (or impedance contrast, if the system operates in the RF range as is the case in Ref. [26]).

With the aim of generating SFL regimes in a linear and passive interferometer, we have explored another alternative. Instead of connecting in series several MZIs, we increase the number of arms of a single interferometer. As a first attempt, we considered a four-beam interferometer with a nominal length difference (Δ) between adjacent arms [28,29]. The system was built with coaxial cables and measurements were performed for narrowband RF pulses centered at the transmission minima (the system exhibits three minima between two main transmission peaks). Simulations in the optical range for a Si-micromachined interferometer were also analyzed [29]. It was found that subluminal propagation only occurred if the length of any of the interferometer's arms was changed in a very small fraction (ξ) of the nominal length difference Δ; otherwise, the pulse propagation regime was tunneling or superluminal.

These results look appealing but there remain open questions: Why is slow light not obtained for a constant length difference between the interferometer's arms? Why is a *small* length detuning ξ in one of the arms necessary to get a fast-slow light transition? Is there a critical value for such detuning? Can we predict, in terms of ξ, at which transmission minimum slow light will arise?

The present paper addresses these questions. Figure 1 shows a schematic that illustrates the concept of a lossless three-arm interferometer showing the typical transmission spectrum. We consider the simplest interferometer (least number of arms N) where a length detuning in a branch implies a change in the otherwise constant length difference between adjacent arms (Δ). Note that this condition holds only for $N \geqslant 3$ (this is why a MZI does not sustain slow light). We develop a model that fully describes SFL effects in such a three-beam interferometer. An exact expression of the group delay as a function of frequency, attenuation, and length detuning is derived. An approximate (but simpler) equation of the group

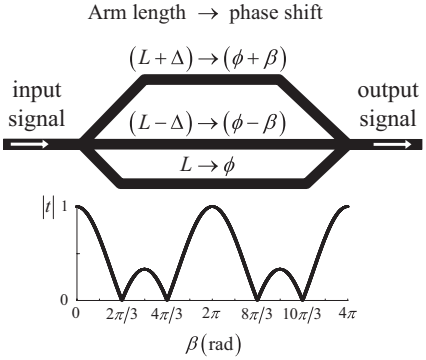

FIG. 1. Schematic of a lossless three-arm interferometer and its typical transmission spectrum.

delay at the transmission minima is given, and the critical length detuning needed to obtain slow light at each minimum is obtained. For the sake of generality, the theoretical results are presented using normalized frequencies and normalized group delays. A proof-of-model experiment is performed in the RF range by using coaxial cables and 1×3 wave splitters.

This work is outlined as follows. In Sec. II the analytical model is developed and its range of validity discussed. Section III describes the experimental techniques used in the proof-of-model experiments performed in the RF range. The results and discussion of such experiments are given in Sec. IV, where the frequency and time-domain characterization of several three-beam RF interferometers is reported and their agreement with theory is discussed. Basic figures of merit of the proposed SFL system and a design in the optical range are discussed. Finally, Sec. V contains the conclusions of this work.

II. ANALYTICAL MODEL

We consider a plane wave, with complex amplitude of 3, impinging on a three-arm interferometer. A 1×3 splitter divides the wave in three equal components that travel along each arm and then recombine by a 3×1 coupler. The transmitted complex amplitude at the end of the interferometer is:

$$t = \sum_{i=1}^{3} e^{j\phi_i}, \tag{2}$$

where ϕ_i is the phase factor of the wave propagating along the ith branch, which, in turn, can be expressed as

$$\phi_i = \frac{\omega}{v} L_i + j\alpha L_i. \tag{3}$$

In Eq. (3) ω is the angular frequency, v is the phase velocity in the medium, L_i is the ith arm length, and α is the attenuation coefficient through the medium, which for simplicity is assumed to be constant over the whole frequency range. We define the length of each arm as:

$$L_1 = L - \Delta(1-\xi), \quad L_2 = L, \quad \text{and} \quad L_3 = L + \Delta, \tag{4}$$

where Δ is the nominal length difference between adjacent arms. A small length detuning ($\xi \ll 1$) in the first arm is introduced to explore the induced transitions in the pulse propagation regimes at the transmission minima. The effective length of the interferometer is, thus [25],

$$L_{\text{eff}} = \frac{(L_1 + L_2 + L_3)}{3} = L + \frac{\xi\Delta}{3}. \tag{5}$$

By defining β as the phase associated to the nominal length difference, Δ, i.e., $\beta = \omega\Delta/v$, the real and imaginary parts of the transmission coefficient can be written as

$$\text{Re} = 1 + e^{-\alpha\Delta}\cos\beta + e^{\alpha\Delta(1-\xi)}\cos[\beta(1-\xi)], \tag{6a}$$

$$\text{Im} = e^{-\alpha\Delta}\sin\beta - e^{\alpha\Delta(1-\xi)}\sin[\beta(1-\xi)]. \tag{6b}$$

And the magnitude and phase of the transmission coefficient can be expressed as

$$|t| = e^{-\alpha L}\sqrt{\text{Re}^2 + \text{Im}^2}, \tag{7a}$$

$$\phi_t = \frac{\beta L}{\Delta} + \arctan\left(\frac{\text{Im}}{\text{Re}}\right). \tag{7b}$$

Let us note that the above quantities depend on ω through β.

We describe the propagation of an electromagnetic pulse through the interferometer in terms of the group delay, which is the time delay of the pulse envelope as it propagates through the system [1]. Following the usually adopted phase-time approach [18,23], the group delay is obtained from the frequency derivative of the transmission coefficient phase:

$$\tau_g = \frac{\partial \phi_t}{\partial \omega} = \frac{L}{v} + \frac{\mathrm{Re}\frac{\partial \mathrm{Im}}{\partial \omega} - \mathrm{Im}\frac{\partial \mathrm{Re}}{\partial \omega}}{\mathrm{Re}^2 + \mathrm{Im}^2}. \tag{8}$$

Therefore, the exact expression of the group delay through the interferometer with constant attenuation α as a function of frequency (through β) and length detuning ξ is then

$$\frac{\tau_g}{\tau_p} = 1 + \frac{\Delta}{L}\frac{e^{-2\alpha\Delta} - (1-\xi)e^{2\alpha\Delta(1-\xi)} + e^{-\alpha\Delta}\cos\beta - (1-\xi)e^{\alpha\Delta(1-\xi)}\cos[\beta(1-\xi)] + \xi e^{-\alpha\Delta\xi}\cos[\beta(2-\xi)]}{1 + e^{-2\alpha\Delta} + e^{2\alpha\Delta(1-\xi)} + 2e^{-\alpha\Delta}\cos\beta + 2e^{\alpha\Delta(1-\xi)}\cos[\beta(1-\xi)] + 2e^{-\alpha\Delta\xi}\cos[\beta(2-\xi)]}. \tag{9}$$

In Eq. (9), the group delay has been normalized by $\tau_p = L/v$, that is, the phase delay in the medium over length L. Next, we analyze particular cases of attenuation and detuning.

A. Interferometer without detuning ($\xi = 0$)

Let us first consider the case where the length difference between adjacent arms is a constant ($\xi = 0$), and thus the interferometer effective length is $L_{\mathrm{eff}} = L$.

1. *Lossless media* ($\alpha = 0$)

In this case, $\mathrm{Re} = 1 + 2\cos\beta$ and $\mathrm{Im} = 0$. This implies that transmission minima are located where $\cos\beta = -1/2$; i.e., the first and second transmission minima after a principal maximum of order m lie at $\beta_1^0 = 2\pi(m + \frac{1}{3})$ and $\beta_2^0 = 2\pi(m + \frac{2}{3})$, respectively. From Eq. (8) it is then trivial to obtain the group delay at the minima as $\tau_g/\tau_p = 1$. The group delay is identical to the phase delay and, consequently, the group velocity equals the phase velocity. Therefore, a lossless interferometer with $\xi = 0$ cannot sustain anomalous propagation regimes. This is not surprising, since in a linear system with nothing altering the phase relation between the pulse components, the pulse peak cannot be shifted and, hence, it travels at the phase speed.

2. *Lossy media* ($\alpha > 0$)

If we consider a certain level of losses ($\alpha > 0$), the transmission minima are located where

$$\cos\beta = -\frac{\cosh(\alpha\Delta)}{2}. \tag{10}$$

Taking this into account, the group delay at the transmission minima according to Eq. (9) will be

$$\frac{\tau_g}{\tau_p} = 1 - \frac{\Delta}{L}\coth(\alpha\Delta). \tag{11}$$

As the coth function is always positive for positive argument values, τ_g/τ_p is always smaller than 1 and, consequently, the system will never sustain subluminal regime. However, tunneling and superluminal regimes can arise at the minima by properly choosing the interferometer effective length for a given attenuation coefficient.

In order to go into more detail, we consider small values of $\alpha\Delta$, for which the transmission minima can be taken to lie at $\beta_{1,2}^0$ (defined in Sec. II A 1) and Eq. (11) can be approximated by:

$$\frac{\tau_g}{\tau_p} \approx \left(1 - \frac{1}{\alpha L}\right). \tag{12}$$

The interferometer will therefore sustain tunneling at the minima ($\tau_g < 0$) if the effective length is chosen so that

$$\alpha L < 1, \tag{13}$$

whereas superluminal regime is possible at the minima ($0 < \tau_g < L/c$) if the effective length satisfies the condition

$$1 < \alpha L < \frac{n}{n-1}, \tag{14}$$

where n is the real part of the medium's refractive index. Two interesting points should be remarked. First, Eqs. (13) and (14) are restrictions on the values of the system's total attenuation. Hence, a proper change in the attenuation range (either by changing α and/or the interferometer's effective length L) could change the propagation regime at the transmission minima. Second, the former conditions do not depend on Δ; the only role of Δ being that of determining the location of the minima.

The behavior discussed above is illustrated by numerical simulations on an interferometer with refractive index $n = 1.5$. Figure 2 shows the transmission coefficient magnitude calculated using Eq. (7a) and the group delay obtained from Eq. (9), for two attenuation values and $\Delta = L/2$. The transmission curve $|t|$ displays the typical three-beam interference pattern, with principal peaks at $\beta = 2\pi m$ (m is the order of the peak) and two minima located in between [30]. In agreement with our previous discussion, no abnormal propagation regimes occur in the lossless interferometer, while in the case of losses with $\alpha\Delta = 0.01$, tunneling appears around the two minima and negative group delays of almost $-50\tau_p$ can be reached.

The evolution of the pulse propagation regime at the minima, as a function of the total system's attenuation αL is described in Fig. 3. We consider $\alpha\Delta = 0.01$and the τ_g curve obtained from Eq. (11) is plotted together with the straight line corresponding to the propagation phase delay through vacuum (L/c). Since the medium's refractive index is 1.5, $L/c = \tau_p/1.5$. As we can see, for small enough attenuation ($\alpha L < 1$) the system exhibits tunneling, in agreement with Eq. (13). For values of αL ranging between 1 and 3, superluminal propagation is sustained, in agreement with Eq. (14), and the system presents normal dispersion if $\alpha L > 3$. Hence, the total

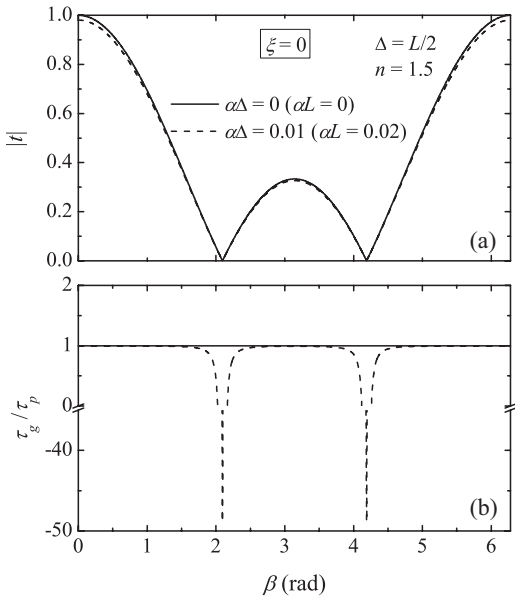

FIG. 2. (a) Transmission coefficient magnitude and (b) group delay Eq. (9) in units of the phase delay through the medium of a three-beam interferometer with length difference between adjacent arms $\Delta = L/2$, length detuning $\xi = 0$, and refractive index $n = 1.5$, for two values of the attenuation coefficient α.

attenuation in the system determines the pulse propagation regime. Fast light is achieved with small enough attenuation while it disappears if it is either too high ($\alpha L > \frac{n}{n-1}$) or zero.

B. Interferometer with detuning ($\xi \neq 0$)

We now consider the case where a small length detuning ($\xi \ll 1$) is introduced in the first branch of the interferometer. If $\alpha\Delta$ and $|\xi|$ are small, it can be shown that the transmission minima move with ξ according to

$$\beta_{1,2} \approx \beta_{1,2}^0 \left(1 + \frac{\xi}{2}\right), \tag{15}$$

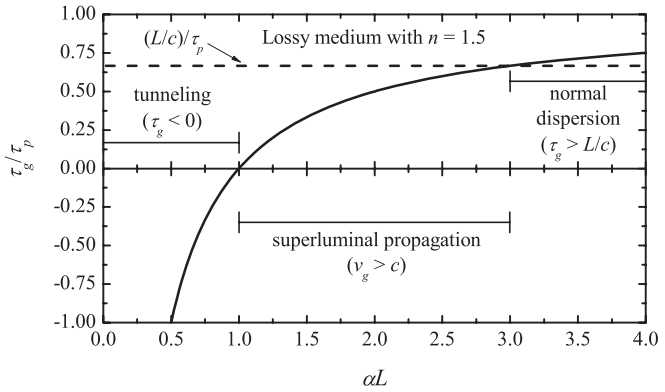

FIG. 3. Pulse propagation regimes at the transmission minima of a lossy three-beam interferometer without detuning ($\xi = 0$) as a function of the total system's attenuation αL. Group delay plotted from Eq. (11) (solid line) and phase delay through vacuum (dashed line). The delays are given in units of the phase delay through the medium.

where $\beta_{1,2}^0$ corresponds to the first and second minima when $\xi = 0$ and $\alpha = 0$.

1. Lossless media ($\alpha = 0$)

In a lossless medium, following Eq. (9), the group delay at the first and second transmission minima can be approximated by

$$\frac{\tau_{g1}}{\tau_p} \approx 1 - \frac{\Delta}{L}\frac{2\sqrt{3}}{\xi\beta_1^0}, \tag{16a}$$

$$\frac{\tau_{g2}}{\tau_p} \approx 1 + \frac{\Delta}{L}\frac{2\sqrt{3}}{\xi\beta_2^0}, \tag{16b}$$

respectively. Consequently, by setting $\xi \neq 0$, one can always obtain slow light at one of the minima. More specifically, these are the possible cases:

(i) If $\xi < 0$, the system sustains slow light at the 1st minimum. At the 2nd minimum, the possible pulse propagation regime is tunneling if

$$L < -\frac{2\sqrt{3}}{\beta_2^0\xi}\Delta, \tag{17}$$

and superluminal ($0 < \tau_g < L_{\text{eff}}/c$) if

$$-\frac{2\sqrt{3}}{\beta_2^0\xi}\Delta < L < -\left(\frac{n}{n-1}\right)\frac{2\sqrt{3}}{\beta_2^0\xi}\Delta. \tag{18}$$

Otherwise, only normal propagation will be possible at the 2nd minimum.

(ii) If $\xi > 0$, slow light occurs at the 2nd minimum, whereas at the 1st minimum, the system will sustain tunneling if

$$L < \frac{2\sqrt{3}}{\beta_1^0\xi}\Delta, \tag{19}$$

and superluminal propagation if

$$\frac{2\sqrt{3}}{\beta_1^0\xi}\Delta < L < \left(\frac{n}{n-1}\right)\frac{2\sqrt{3}}{\beta_1^0\xi}\Delta. \tag{20}$$

Otherwise, only normal propagation occurs at the 1st minimum. The above expressions set restrictions on the length L of the second branch, which is very close, but not equal, to the system's effective length [see Eq. (5)].

This behavior is observed in Fig. 4, for a three-arm interferometer, where its first branch has been increased or decreased according to $\xi = \pm 5\%$. Exact Eq. (9) was used to simulate the group delay as a function of β in a system with $\Delta = L/2$ and refractive index $n = 1.5$. The transmission's minima shift with ξ is manifest in the group delay curves. According to the approximation in Eq. (16), for a detuning of $+5\%$, the group delay should be $-15.5\tau_p$ and $9.3\tau_p$ at the first and second minima of zero-order, respectively. Whereas, if $\xi = -5\%$, the expected group delay at the zero-order first and second minimum is $17.5\tau_p$ and $-7.3\tau_p$, respectively. These approximate values of the group delay at the minima are in excellent agreement with the exact results shown in the figure.

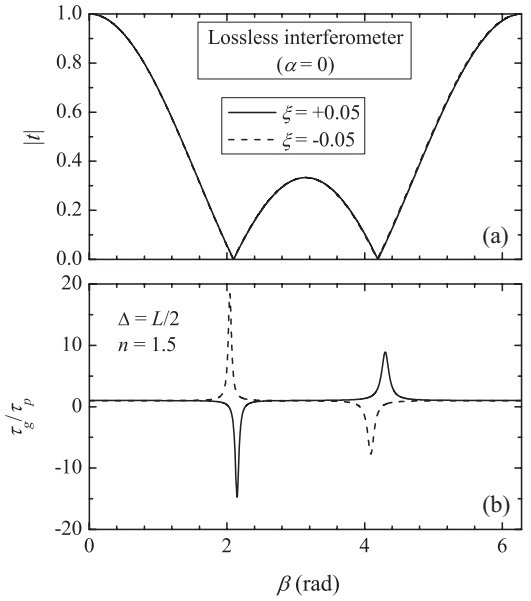

FIG. 4. (a) Transmission coefficient magnitude and (b) group delay of a lossless three-beam interferometer with nominal length difference between adjacent arms $\Delta = L/2$ and refractive index $n = 1.5$, for two values of length detuning ξ.

2. *Lossy media ($\alpha > 0$)*

In the most general case, where both detuning and a certain attenuation level are considered, and under the conditions of small $\alpha\Delta$ and $|\xi|$, Eq. (9) can be approximated at the transmission minima as

$$\frac{\tau_{g1}}{\tau_p} \approx 1 - \frac{\Delta}{L}\frac{2\sqrt{3}}{\beta_1^0(\xi - \xi_{c1})}, \tag{21a}$$

$$\frac{\tau_{g2}}{\tau_p} \approx 1 + \frac{\Delta}{L}\frac{2\sqrt{3}}{\beta_2^0(\xi - \xi_{c2})}, \tag{21b}$$

where the critical detuning lengths ξ_{c1} and ξ_{c2} are approximately

$$\xi_{c1} = -\frac{2\sqrt{3}\alpha\Delta}{\beta_1^0}, \tag{22a}$$

$$\xi_{c2} = +\frac{2\sqrt{3}\alpha\Delta}{\beta_2^0}. \tag{22b}$$

For lossless media, $\xi_{c1} = \xi_{c2} = 0$ and Eqs. (21) reduce to Eqs. (16); thus, recovering the situation discussed in Sec. II B 1. The role of the attenuation is then to increase the magnitude of the critical detuning needed to obtain slow light at the minima. Table I summarizes the possible propagation regimes at both minima. If $\xi < \xi_{c1}$, the system only sustains slow light at the 1st minimum. If $\xi > \xi_{c2}$, the system only sustains slow light at the 2nd minimum. For $\xi_{c1} < \xi < \xi_{c2}$ the allowed pulse propagation regimes at the minima can be tunneling, superluminal, or normal, depending on the length L. Table II summarizes the possible propagation regimes at the 1st minimum. If $\xi > \xi_{c1}$, there is a maximum value of L to obtain tunneling at the 1st minimum:

$$L_{t1} = \left(\alpha + \frac{\beta_1^0\xi}{2\sqrt{3}\Delta}\right)^{-1}. \tag{23}$$

For lengths L greater than L_{t1} and smaller than $(\frac{n}{n-1})L_{t1}$, superluminal propagation is sustained at the 1st minimum. Finally, when L exceeds the value $(\frac{n}{n-1})L_{t1}$, the normal regime is attained.

Similarly, the possible propagation regimes at the 2nd minimum are shown in Table III. For $\xi < \xi_{c2}$, there is a maximum value of L to get tunneling at the 2nd minimum:

$$L_{t2} = \left(\alpha - \frac{\beta_2^0\xi}{2\sqrt{3}\Delta}\right)^{-1}. \tag{24}$$

For lengths greater than L_{t2} and smaller than $(\frac{n}{n-1})L_{t2}$, superluminal propagation occurs at the 2nd minimum. Once again, when L exceeds the value $(\frac{n}{n-1})L_{t2}$ the normal regime is attained. In the case $\xi = 0$, lengths $L_{t1} = L_{t2} = 1/\alpha$, and Eqs. (13) and (14), for a lossy interferometer with a constant length difference Δ between adjacent branches, are recovered. Let us remark that, as opposed to that case, Δ does now influence the conditions that determine the propagation regime.

We have checked the validity of the approximated Eqs. (21) and (22) for estimating the group delay at the transmission minima. The approximated value has been compared with the exact result obtained from Eq. (9), as a function of the detuning ξ and for an attenuation level of $\alpha\Delta = 0.01$. The results in Fig. 5 reveal the following features: (i) the agreement between the approximated and the exact value of τ_g is excellent for ξ up to $\pm 5\%$; (ii) the group delay increases in magnitude as the detuning approaches the critical value; and (iii) the SFL transition when reaching the critical detuning is extremely abrupt. Namely, the absolute value of τ_g at each minimum approaches infinity when the length detuning equals exactly the corresponding ξ_c. This behavior is understood from

TABLE II. Possible propagation regimes at the 1st transmission minimum.

Condition	$L < L_{t1}$	$L_{t1} < L < (\frac{n}{n-1})L_{t1}$	$L > (\frac{n}{n-1})L_{t1}$
$\xi < \xi_{c1}$	Slow	Slow	Slow
$\xi > \xi_{c1}$	Tunnel.	Superlum.	Normal

TABLE I. Possible propagation regimes at the transmission minima.

Condition	Regime at 1st min	Regime at 2nd min
$\xi < \xi_{c1}$	Slow	Tunnel., Superlum., and Normal
$\xi_{c1} < \xi < \xi_{c2}$	Tunnel., Superlum., and Normal	Tunnel., Superlum., and Normal
$\xi > \xi_{c2}$	Tunnel., Superlum., and Normal	Slow

TABLE III. Possible propagation regimes at the 2nd transmission minimum.

Condition	$L < L_{t2}$	$L_{t2} < L < (\frac{n}{n-1})L_{t2}$	$L > (\frac{n}{n-1})L_{t2}$
$\xi < \xi_{c2}$	Tunnel.	Superlum.	Normal
$\xi > \xi_{c2}$	Slow	Slow	Slow

Eqs. (6)–(8): for a given $\alpha\Delta$ value, the critical detuning is the one that makes $\mathrm{Re}^2 + \mathrm{Im}^2 = 0$ at the corresponding minimum. Therefore, this abrupt SFL transition is achieved through a passage from a zero transmission condition. We would like to draw attention here to the similarity of this mechanism with that reported by Longhi in active fiber Bragg gratings with asymmetric profile [17]. In that work, an abrupt superluminal to subluminal transition of reflected pulses near to a local minimum of the reflection spectrum is achieved by increasing the gain level.

III. EXPERIMENTAL TECHNIQUES

In this section, the experimental setup we have used for our proof-of-model experiment is described. We have designed a nominal interferometer consisting of a 1×3 RF power splitter, a 3×1 RF coupler (both PE2002, Pasternack), and three coaxial cables (50 Ω, RG-58C/U). The designed effective length of the system is 2 m and the intended length difference between adjacent cables is 1 m. In practice, every branch of the interferometer comprises the cable itself, the connectors between cable and splitters, and a small track inside the splitters. After measuring all these elements, the actual branch lengths of the starting interferometer were found to be $L_1 = 1.049$ m, $L_2 = 2.066$ m, and $L_3 = 3.088$ m, yielding $\Delta = 1.022$ m, and $\xi = +0.5\%$, according to our definitions in Eq. (4). In addition, four coaxial cables were prepared to substitute the L_1 cable of the starting interferometer. The actual first arm lengths are 0.989, 1.008, 1.086, and 1.103 m. Therefore, we have five interferometers to be characterized in frequency and time domain, each with $\Delta = 1.022$ m, and a set of values for ξ of -5.4%, -3.5%, $+0.5\%$, $+4.1\%$, and $+5.8\%$.

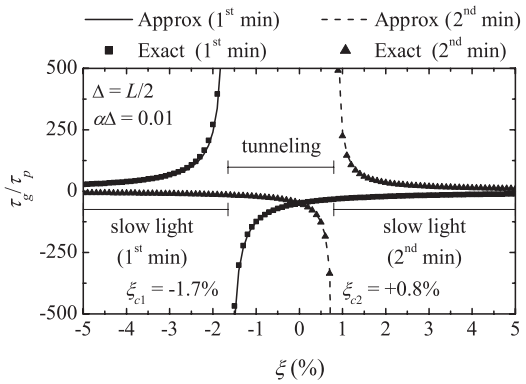

FIG. 5. Dependence with length detuning of the group delay at the minima for a three-beam interferometer with nominal length difference between adjacent arms $\Delta = L/2$ and attenuation $\alpha\Delta = 0.01$. The approach in Eqs. (21) (line) is compared to the exact result of Eq. (9) (symbols) for each minima.

TABLE IV. Fabricated three-beam RF interferometers with $L = 2.066$ m, $\Delta = 1.022$ m.

Interferometer	L_1 (m)	ξ(%)
L1-99	0.989	−5.4
L1-101	1.008	−3.5
L1-105	1.049	+0.5
L1-109	1.086	+4.1
L1-110	1.103	+5.8

This set of ξ values allows checking the evolution from fast to slow light at the minima as L_1 varies. All the cables available for the branches were cut out of the same long coaxial cable whose attenuation coefficient as a function of frequency, $\alpha(\omega)$, had been previously determined following the procedure in Ref. [30]. Knowing the system's attenuation was necessary in order to estimate the critical length detuning through Eq. (22) so that we could prepare the cables with adequate values of ξ to display the SFL transition. From the characterization of $\alpha(\omega)$ we obtained an attenuation of $\alpha = 0.015$ Np/m (0.13 dB/m) at 65.2 MHz (first transmission minimum of the nominal interferometer) and $\alpha = 0.022$ Np/m (0.19 dB/m) at 130.4 MHz (second transmission minimum of the nominal interferometer). These attenuation values yield a critical length detuning of $\xi_{c1} = -2.5\%$ and $\xi_{c2} = +1.9\%$ for the first and second minimum, respectively. The characteristics of the fabricated RF three-beam interferometers are summarized in Table IV.

The frequency characterization of these interferometers has been performed by means of a two-port vector network analyzer (PNA series, Agilent E8363B). The scattering parameter S_{21} (the transmission coefficient) was recorded in the 10–200 MHz range every 59.375 kHz with an average of 64 to help suppress the random noise. In addition, a full characterization of the splitters was carried out. We use this measurement to correct the interferometer experimental response for a proper comparison with simulation, which does not include the effect of the splitters. It was shown that both splitters directly interconnected introduce an overall group delay of 1.8 ns and an attenuation of 1 dB, approximately, in the transmission response.

The experimental data contain a small amount of noise, which is not very apparent in the S_{21} parameter itself. To obtain the experimental group delay, the phase data curve is differentiated and this amplifies the noise leading to spurious effects. For this reason, the network analyzer was configured to smooth the group delay by averaging 17 adjacent points. Although it is well known that smoothing may give results which vary critically with the smoothing parameters, the selected averaging algorithm preserves the key features of the group delay at the transmission minima.

Additionally, time-domain pulse propagation experiments have been performed on each interferometer. The experimental set-up is shown in Fig. 6. The 300 kHz sinusoidal output of generator-1 (Tektronix CFG-253) is used to amplitude modulate the sinusoidal signal of generator-2 (IntraAction VFE-604A4), whose frequency can be varied between 40 and 80 MHz. Therefore, only the first minimum can be observed. This produces a train of 3.3-μs-wide sinusoidally modulated

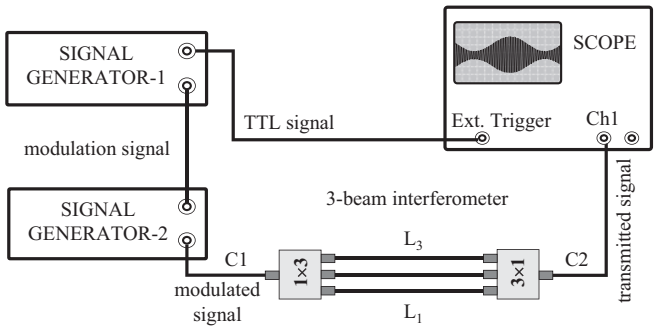

FIG. 6. Experimental set-up for the time-domain pulse propagation measurements through the RF interferometers. The output sinusoidal signal from generator-2 is 100% amplitude modulated by the output signal from generator-1. C1 and C2 are 50 Ω coaxial cables constituting the reference path (see text).

wave packets with carrier frequencies in the MHz range. The pulse train transmitted through the interferometer is recorded at the oscilloscope (Agilent DSO-6032A) with a resolution of 0.5 ns (10 kSamples/5000 ns). The TTL signal from generator-1 is used to trigger the oscilloscope.

The group delay for each C1-interferometer-C2 system (see Fig. 6) was estimated by the following procedure: first, a capture of the transmitted pulses was taken for a carrier frequency coinciding with the interferometer's 1st transmission minimum. Next, the interferometer was removed and cable C1 was connected to cable C2, and captures of transmitted pulses through this reference assembly were performed at the same carrier frequency than before. For each interferometer, the group delay is then estimated as the time shift between the peak of the pulse transmitted by the system and the peak of the pulse traveling through the reference path. Let us recall that the group delay estimated in this way will approach to the one retrieved from Eq. (8) as the modulation frequency decreases.

IV. RESULTS AND DISCUSSION

This section discusses the experimental results obtained for the fabricated RF interferometers described in Sec. III. Frequency and time-domain measurements were performed on these systems. The results are compared with the theoretical model developed in Sec. II. A design of such a device in the optical range is also proposed and discussed.

A. Results in the frequency domain

Figures 7 and 8 show the transmission (magnitude $|t|$ and phase ϕ_t) and group delay (τ_g) of our five three-beam RF interferometers whose parameters are summarized in Table IV. Experimental and simulation results are shown. Namely, we include two experimental curves. One corresponds to the whole system measured with the vector network analyzer (labeled *uncorrected experimental data*)—including the splitters—while the other (labeled *corrected experimental data*) is the result of subtracting the effect of the splitters in the way indicated in Sec. III. For each interferometer, the simulated $|t|$ and ϕ_t curves were obtained as in Ref. [30], by numerically calculating the interference of three sinusoidal RF

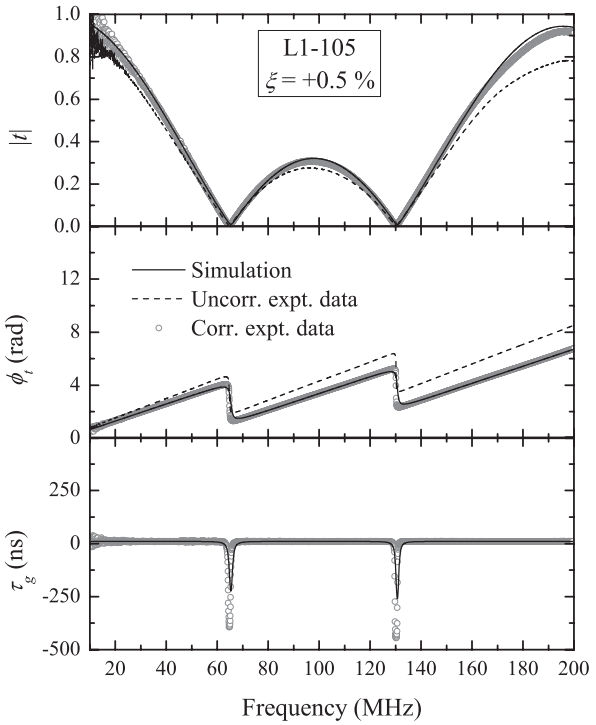

FIG. 7. Numerical simulation (solid curve) and experimental frequency-domain characterization of the starting interferometer L1-105. The dashed curve corresponds to the whole system measured with the vector network analyzer—including the splitters—and the symbols refer to the result of subtracting the effect of the splitters in the way indicated in Sec. III. (a) Magnitude of the transmission coefficient, (b) phase of the transmission coefficient, and (c) 17-point averaged group delay.

waves propagating through coaxial cables of the lengths given in Table IV, including the frequency-dependent attenuation in the cables. The τ_g curves were obtained by differentiating the corresponding numerical phase curve with respect to the frequency. The same 17-point smoothing algorithm as that applied to the measured τ_g curve was used for the simulated group delay. The agreement between simulations and the corrected experimental results is very good, thus assessing the accuracy of the procedure employed to subtract the effect of the splitters. From the figures, it is obvious that the splitters introduce losses (the peaks in transmission are less pronounced for the raw data) and also they add an additional phase (the raw data phase function is above the numerical one). Their effect on the group delay is hardly noticeable; for this reason only the corrected experimental τ_g curve is shown in the figures.

Let us first analyze the situation for the starting interferometer L1–105, which is displayed in Fig. 7. The $|t|$ curves exhibit absolute maxima every 200 MHz and two minima between the zero and the first-order principal peak that lie close to the expected positions $f_{01} = 65.4$ MHz and $f_{02} = 130.8$ MHz [see Eq. (15)]. Negative group delay around -400 ns are reached at both minima, accordingly to the steep negative slope of the phase function at these frequencies. These results agree with our model predictions, since the interferometer's length detuning ($+0.5\%$) satisfies the condition $\xi_{c1} < \xi < \xi_{c2}$ (with $\xi_{c1} = -2.5\%$, and $\xi_{c2} = +1.9\%$), and the length of the second

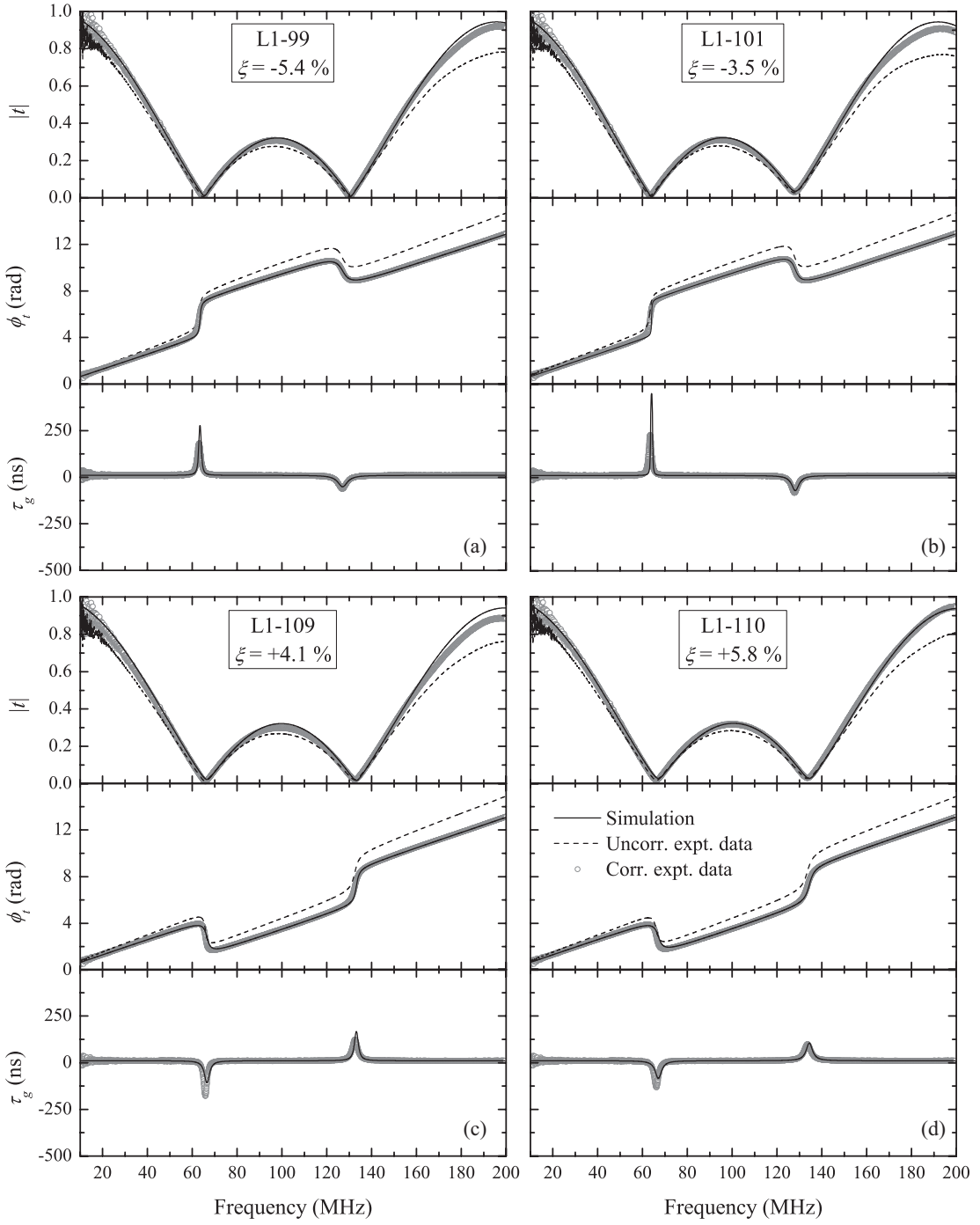

FIG. 8. Numerical simulations (solid curve), uncorrected (dashed curve), and corrected (symbols) experimental results for the frequency-domain characterization of three-beam RF interferometers. Top panel shows magnitude of the transmission coefficient, middle panel shows phase of the transmission coefficient, and bottom panel shows the 17-point averaged group delay for samples (a) L1-99, (b) L1-101, (c) L1-109, and (d) L1-110.

branch ($L = 2.066$ m) is well below the limiting values ($L_{t1} = 55.7$ m and $L_{t2} = 62.2$ m) above which tunneling regime disappears.

Figure 8 shows how the situation changes when the interferometer's length is slightly changed. According to theory, a reduction of at least $2.5\%\Delta$ in branch length L_1 fulfills the condition to generate slow light at the 1st minimum. On the contrary, an increase of at least $1.9\%\Delta$ would generate slow light at the 2nd minimum. Figures 8(a)–8(d) correspond to samples L1-99, L1-101, L1-109, and L1-110, respectively. In the two samples with shorter L_1, the system exhibits positive τ_g at the 1st minimum, while negative τ_g is retained at the 2nd minimum. The opposite situation occurs for samples L1-109 and L1-110. These results are justified within our model, considering the length detuning ξ of each sample (Table IV), the critical detuning lengths (ξ_{c1}, ξ_{c2}), and the model conditions

summarized in Tables II and III. Namely, $\xi < \xi_{c1} = -2.5\%$ for the system in Figs. 8(a) and 8(b) and $\xi > \xi_{c2} = +1.9\%$ for the system in Figs. 7(c) and 7(d), which explains the occurring of slow light at the 1st minimum in one case and at the 2nd minimum in the other. Also, a quick estimation using Eq. (24) shows that only tunneling can be sustained at the 2nd minimum for interferometers L1-99 and L1-101, since L (2.066 m) is for both systems smaller than L_{t2} (11.6 m and 15.8 m, respectively). A similar result occurs by using Eq. (23) to obtain the value of L_{t1} for systems L1-109 and L1-110; we find $L < L_{t1}$ (25.5 m, and 20.3 m, respectively), and this is why these samples exhibit tunneling at the 1st minimum.

From Fig. 8, the link between the strength of the group delay peaks and the steepness in the slope of the phase function is obvious. Such steepness is ultimately linked to the attenuation in the system (for higher attenuations the slopes are less pronounced) and to how much ξ approaches the critical detuning ξ_{c1} or ξ_{c2}. Samples L1-101 and L1-105 are the ones with ξ closer to one of the critical values, thus leading to the highest and narrowest τ_g peaks. Finally, the frequency shift of the minima as the length detuning varies is evident in Fig. 8. The minima move toward higher frequency as ξ increases, just like the theoretical model predicts.

B. Results in the time domain

Pulse propagation experiments were carried out using the experimental setup described in Sec. III (Fig. 6). The modulating signal was a 300 kHz sinusoidal wave, which results in a 3.3-μs-wide pulse. This choice of the modulating frequency was a compromise between narrow-enough bandwidth to avoid pulse distortion and large-enough bandwidth to get appreciable pulse peak advancements (or delays) in comparison to the pulse length. For each interferometer, the carrier frequency was selected to coincide with the first transmission's minimum. Since the signals were largely attenuated, a direct observation of the pulse peak on the oscilloscope was not accurate enough to measure the group delay. Hence, the pulse peak position was obtained from a numerical analysis of the data by finding the best fit to the pulse envelope.

Figure 9 shows the pulse captures for the five RF interferometers. The arrow indicates the time spent by the pulse peak in propagating through the interferometers and it is obtained as explained in Sec. III. The SFL transition in the pulse propagation regime is evident in these captures. The τ_g values agree reasonably well with those found in the frequency-domain characterization. The pulse propagates with negative group delay of -302, -147, and -115 ns in samples L1-105, L1-109, and L1-110, respectively. Whereas positive group delays of $+248$ and $+308$ ns occur in samples L1-99, and L1-101, respectively. As it is clearly demonstrated in Refs. [31–33], such peak advancements and delays arise from the coherent interference of the pulse frequency components. Each component travels at phase velocity $2/3c$ in the cables, but their relative phases are modified after the pulse's transmission through the system; as a result, the peak of the output pulse (where the frequency components are all in phase) is shifted backward (or forward) and the pulse appears to travel at superluminal (or subluminal) speed. As it is argued in several works [32,33], these abnormal propagation regimes

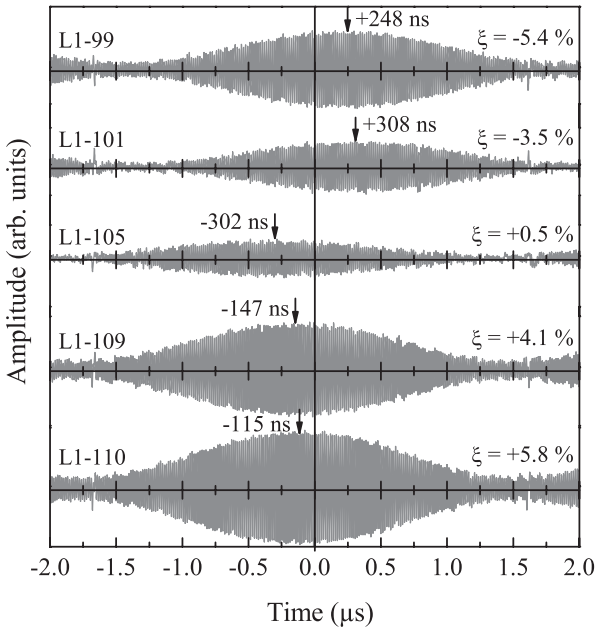

FIG. 9. Wave-packet traces of the RF interferometers (from top to bottom) L1-99, L1-101, L1-105, L1-109, and L1-110. In each case, the pulse carrier frequency is that of the 1st transmission minimum. The arrow indicates the pulse propagation time through the interferometer and it is obtained as mentioned in Sec. III.

occur only if the spatial length of the pulse (L_{pulse}) greatly exceeds that of the system. This condition is nicely satisfied here, since $L_{\text{pulse}} = 3.3\ \mu\text{s} \times 2/3c = 400$ m is much longer than the interferometer's length ($L_{\text{eff}} \approx 2$ m).

C. Further discussion and operation in the optical range

Let us now discuss some figures of merit of the three-beam interferometer as an SFL system and its possible realization for delaying or advancing optical pulses. Considering an interferometer with a small length detuning, ξ, simulations show that the relative group delay $|\tau_{\text{del}}| = \tau_g - \tau_p$, which is the difference between the group delay and the phase delay in the medium over length L, matches a sequence of Lorentzian functions centered at each transmission minimum:

$$|\tau_{\text{del}}| = \frac{1}{2\pi} \frac{\frac{\Gamma}{2}}{(f - f_{\text{min}})^2 + \left(\frac{\Gamma}{2}\right)^2}, \tag{25}$$

where f_{min} is the frequency of the considered transmission minimum and Γ is the full width at half maximum (FWHM) of the Lorentzian function at that minimum. The maximum relative group delay is then $|\tau_{\text{del}}|_{\text{peak}} = 1/\pi\Gamma$. Since the pulse delay (or advancement) will only be effective for signals centered at the transmission minima and with spectral components within these Lorentzian peaks, the product $|\tau_{\text{del}}|_{\text{peak}} \times \Gamma = 1/\pi \approx 32\%$ gives a rough estimation of the maximum delay-bandwidth product that can be achieved with this system. Let us note that this estimation is valid for any frequency range the interferometer may operate.

Another figure of merit in SFL systems is the fractional delay, defined as the ratio between the relative pulse delay, τ, and the pulse duration, T_0. In our time-domain experiments, we have measured a maximum relative pulse delay of $\sim$300 ns

($\tau_p \sim 10$ ns is almost negligible in comparison). Various measures of the pulse duration are considered by the authors. For our sinusoidally modulated wavepackets and by considering T_0 as the period of the modulating signal (3.3 μs), we obtain a fractional delay of ∼9%. Instead, if we take T_0 as the FWHM of the pulse *amplitude* signal, this parameter becomes ∼18%. Furthermore, by regarding T_0 as the FWHM of the pulse *power* signal, then the measured fractional delay becomes ∼25%. For the rest of the discussion we will consider this last definition of T_0 since it is the optical power, and not the optical field envelope, which is detected in experiments performed in the optical range.

We have also performed numerical simulations on the propagation of sinusoidally modulated pulses through the interferometer. This study shows that the transmitted pulse width, T_{0t}, is smaller than T_0, yielding a pulse compression b, given by $b = 1 - T_{0t}/T_0$. Either pulse delay or advancement is accompanied by a certain degree of pulse compression. The relation between pulse compression and fractional delay is roughly quadratic and for sinusoidally modulated pulses reads

$$b \approx 0.7 \left(\frac{|\tau|}{T_0} \right)^2 . \tag{26}$$

This means that, in order to maintain the pulse compression below 5%, the fractional delay cannot exceed 27%, and to keep it below 10%, the fractional delay cannot exceed 38%. This explains the low pulse compression observed in our measurements with a 300 kHz modulating signal. Time-domain measurements with 500 kHz modulation frequency (not shown here) were carried out to confirm not only a high pulse compression but also a strong distortion.

The above discussion is entirely applicable to three-arm interferometers fabricated to operate at optical frequencies. Leaving the free-space configurations aside, there are several technologies to realize a wave-guided three-arm interferometer operating in the optical range, namely, all-fiber and channel waveguide structures. For practical purposes, it would be desirable to induce the SFL transitions by changing the optical path without affecting the physical length of the arms, i.e., by changing the refractive index. With this idea, lithium niobate (LN) is an excellent candidate material, being an established choice for electro-optic applications such as the realization of Mach-Zehnder optical modulators [34]. Optical waveguides can be fabricated, among other techniques, by in-diffusion of Titanium into an x- or z-cut LN crystal. A precise control of the phase shift in one arm can be achieved by applying an electric field through the metallic electrode above the corresponding

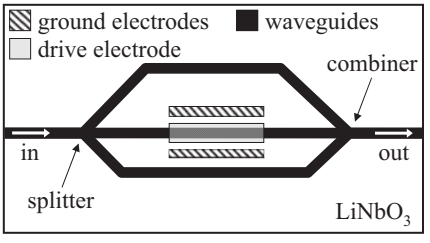

FIG. 10. Schematic of a lithium niobate three-arm interferometer.

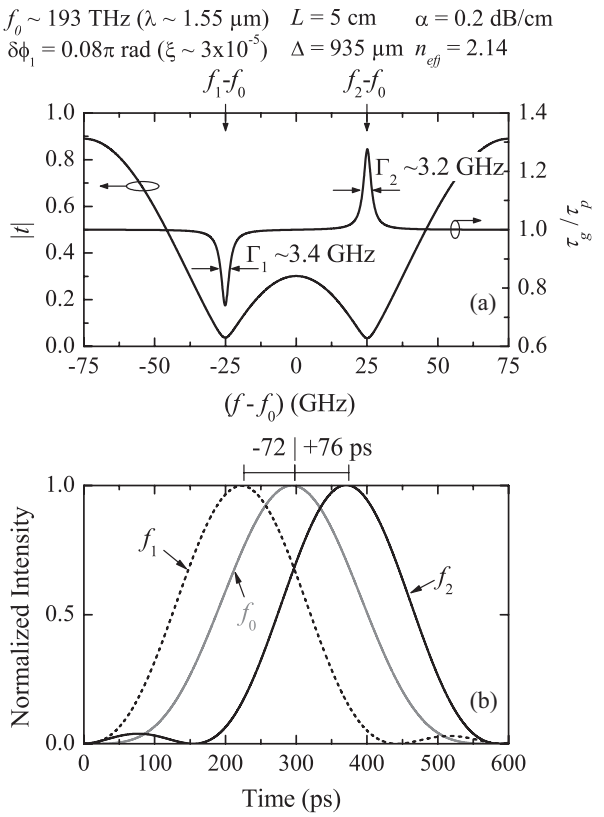

FIG. 11. Numerical simulation of a LN interferometer with the indicated parameters. (a) Magnitude of the transmission coefficient and group delay and (b) pulse traces of transmitted pulses with the indicated carrier frequencies corresponding to different propagation regimes.

waveguide, which induces a refractive index change due to the electro-optic properties of this material. Figure 10 shows a schematic of a z-cut LN unbalanced three-arm interferometer. Although it seems more adequate to place the drive electrode above one of the outer arms, the drive electrode has been placed above the middle arm in order to directly extrapolate our previous analysis with length detuning ξ. Therefore, an external voltage applied to the drive electrode will produce a phase shift, $\delta\phi_1$, in the shortest arm, which is equivalent to introducing a length detuning of $\xi = \frac{c}{n_{\text{eff}} 2\pi f} \frac{\delta\phi_1}{\Delta}$, where n_{eff} is the waveguide effective refractive index.

As an example, let us consider the case of a LN interferometer with $L = 5$ cm, nominal Δ of 935 μm, and a phase shift $\delta\phi_1 \approx 0.08\pi$ rad (equivalent to a length detuning of $\xi = 3 \cdot 10^{-5}$). This value of Δ is chosen so that the separation between transmission minima of the same order is 50 GHz. Figure 11(a) shows the transmission coefficient and the group delay in a frequency range of 150 GHz centered at the middle frequency between a pair of minima of the same order at ∼193 THz. Considering $n_{\text{eff}} = 2.14$, the phase delay in this system is $\tau_p \approx 356$ ps. Fast light regime is sustained at the first transmission minimum, whereas slow light appears at the second minimum. As indicated in the figure, pulses of bandwidth smaller than 3.4 and 3.2 GHz would be required to observe such peak advancement or delay, respectively. We have simulated the propagation of an optical pulse train through this

interferometer. An optical carrier of ∼193 THz ($\lambda = 1.55\ \mu$m) is sinusoidally modulated in order to produce a train of pulses with $T_0 = 214$ ps at a repetition rate of 1.7 GHz. Figure 11(b) shows the pulse traces corresponding to propagation at both transmission minima together with a pulse trace propagating at the central frequency, for which the group delay is τ_p. The relative pulse delays at the first and second minima are ∼−72 ps and +76 ps, respectively, yielding fractional delays of −34% and +36%, with pulse compression of 8% and 9%, respectively. These values are larger than those reported in passive fiber Bragg gratings [16], where fractional delays and advancements of 17% where measured when tuning a picosecond optical pulse spectrum through the grating band gap. Our results are also similar to the ones reported in Ref. [17] for active fiber Bragg gratings when keeping the pulse compression in our system below 13%.

V. CONCLUSIONS

To summarize, we have demonstrated the arising of slow and fast light in linear and passive three-beam interferometers for frequencies close to the transmission minima. Transitions in the pulse propagation regime at these frequencies in terms of the system's characteristics (attenuation and length difference between adjacent arms) were theoretically analyzed. We have proved that slow light is not possible when the length difference between adjacent arms is a constant. In this case, fast light is achieved only if the system has attenuation. The total attenuation drives the group delay transitions at the transmission minima, where tunneling is the expected regime for low total attenuation, whereas superluminality and eventually normal propagation are attained as total attenuation further increases.

By introducing a small length detuning (ξ) in a branch, we have demonstrated that slow light can arise. Analytical expressions for the group delay τ_g at the transmission minima in the approximation of low attenuation and small length detuning were derived, and a critical length detuning (ξ_c) beyond which slow light appears was obtained. We found that in the case of lossless media ξ_c is zero, being the role of the attenuation to increase the magnitude of ξ_c. For every pair of minima located between absolute peaks of the transmission spectra, only one minimum may support slow light at a time, whereas the other minimum will sustain either tunneling, superluminal, or normal dispersion, depending on the system's length.

Let us remark that such length-detuning-driven SFL transition stems from a structural change in the system's dispersive properties at the transmission minima. This change is triggered by the passage through a local zero transmission when the critical detuning value is reached. This is in formal analogy to previously reported group delay tuning mechanism for pulses reflected on active Bragg gratings by changing the gain. But unlike it, here the SFL transition is attained in an entirely passive system.

An experimental demonstration of the model predictions on the pulse propagation regimes has been performed in the RF range by using 50-Ω coaxial cables and 1×3 power splitters to build five interferometers with ξ values ranging from −5.4 to +5.8%. The structures were characterized in the frequency domain, and the group delay at the transmission minima showed the trends predicted by the analytical expressions. The same structures were used in a time-domain setup, where a group delay from less than −300 ns to more than +300 ns was measured for a train of 3.3-μs-wide sinusoidally modulated wavepacket with carrier frequency at the first minimum of each interferometer.

The maximum delay-bandwidth product of the system is estimated to be 32%. Numerical simulations on pulse propagation show that the achievable fractional group delays can reach 38% keeping pulse compression below 10%. These characteristics are intrinsic to the system; i.e., they are independent of its operational frequency range. Therefore, the achievable pulse advancements or delays for small pulse compression are shorter than the pulse duration. This would be a drawback for developing practical delay lines or optical buffers based on this system for signal processing. However, the very abrupt SFL transition when approaching the critical length detuning opens the door for sensing applications. With this sensing scope, let us note that similar phenomena would be expected by varying whatever changes the *optical path* in one of the arms. As an example, a lithium niobate interferometer operative at 1.55 μm was proposed where a fine control of the phase shift in a branch could be achieved by applying an electric field through a metallic electrode, which induces a refractive index change on the waveguide.

ACKNOWLEDGMENTS

Financial support from Ministerio de Educación y Ciencia through Project No. FIS2009-13955-C02-02 is acknowledged. The authors thank Guillermo Martínez de la Torre for the preparation of the coaxial cables.

[1] L. Brillouin, *Wave Propagation and Group Velocity* (Academic Press, New York, 1960).
[2] L. Thévenaz, Nat. Photonics **2**, 474 (2008).
[3] T. F. Krauss, Nat. Photonics **2**, 448 (2008).
[4] E. Cabrera-Granado and D. J. Gauthier, Opt. Pura Apl. **41**, 313 (2008).
[5] R. W. Boyd and P. Narum, J. Mod. Opt. **54**, 2403 (2007).
[6] L. V. Hau, S. E. Harris, Z. Dutton, and C. H. Behroozi, Nature (London) **397**, 594 (1999).
[7] L. J. Wang, A. Kuzmich, and A. Dogariu, Nature (London) **406**, 277 (2000).
[8] A. V. Turukhin, V. S. Sudarshanam, M. S. Shahriar, J. A. Musser, B. S. Ham, and P. R. Hemmer, Phys. Rev. Lett. **88**, 023602 (2001).
[9] M. S. Bigelow, N. N. Lepeshkin, and R. W. Boyd, Science **301**, 200 (2003).
[10] J. Mork, R. Kjaer, M. van der Poel, and K. Yvind, Opt. Express **13**, 8136 (2005).

[11] H. Su and S. L. Chuang, Appl. Phys. Lett. **88**, 61102 (2006).
[12] A. Schweinsberg, N. N. Lepeshkin, M. S. Bigelow, R. W. Boyd, and S. Jarabo, Europhys. Lett. **73**, 218 (2006).
[13] M. González-Herráez, K. Y. Song, and L. Thévenaz, Appl. Phys. Lett. **87**, 081113 (2005).
[14] D. Dahan and G. Eisenstein, Opt. Express **13**, 6234 (2005).
[15] J. F. Galisteo-López, M. Galli, A. Balestreri, M. Patrini, L. C. Andreani, and C. López, Opt. Express **15**, 15342 (2007).
[16] S. Longhi, M. Marano, P. Laporta, and M. Belmonte, Phys. Rev. E **64**, 055602(R) (2001).
[17] S. Longhi, Phys. Rev. E **72**, 056614 (2005).
[18] G. Nimtz, IEEE J. Sel. Top. Quantum Electron. **9**, 79 (2003).
[19] M. Mojahedi, E. Schamiloglu, F. Hegeler, and K. J. Malloy, Phys. Rev. E **62**, 5758 (2000).
[20] A. Sánchez-Meroño, J. Arias, and M. M. Sánchez-López, IEEE J. Quantum Electron. **46**, 546 (2010).
[21] A. Haché and L. Poirier, Phys. Rev. E **65**, 036608 (2002).
[22] J. N. Munday and W. M. Robertson, Appl. Phys. Lett. **83**, 1053 (2003).
[23] M. Kitano, T. Nakanishi, and K. Sugiyama, IEEE J. Sel. Top. Quantum Electron. **9**, 43 (2003).
[24] H. Aynaou, E. H. El Boudouti, Y. El Hassouani, A. Akjouj, B. Djafari-Rouhani, J. Vasseur, A. Benomar, and V. R. Velasco, Phys. Rev. E **72**, 056601 (2005).
[25] M. M. Sánchez-López, A. Sánchez-Meroño, J. Arias, J. A. Davis, and I. Moreno, Appl. Phys. Lett. **93**, 074102 (2008).
[26] E. H. El Boudouti, N. Fettouhi, A. Akjouj, B. Djafari-Rouhani, A. Mir, J. O. Vasseur, L. Dobrzynski, and J. Zemmouri, J. Appl. Phys. **95**, 1102 (2004).
[27] Z. Shi, R. W. Boyd, D. J. Gauthier, and C. C. Dudley, Opt. Lett. **32**, 915 (2007).
[28] A. Sánchez-Meroño, M. M. Sánchez-López, J. Arias, and J. A. Davis, Opt. Pura Apl. **42**, 215 (2009).
[29] A. Sánchez-Meroño, M. M. Sánchez-López, J. Arias, J. A. Davis, and I. Moreno, SPIE Proc. **7716**, 77161Y 1-10 (2010).
[30] J. A. Davis, D. A. Miller, M. M. Sánchez-López, and J. Cos, Am. J. Phys. **74**, 1066 (2006).
[31] L. G. Wang, N. H. Liu, Q. Lin, and S. Y. Zhu, Phys. Rev. E **68**, 066606 (2003).
[32] W. Guo, Phys. Rev. E **73**, 016605 (2006).
[33] O. A. Peverini, R. Tascone, G. Addamo, G. Virone, and R. Orta, IEEE Antennas Wirel. Propag. Lett. **7**, 101 (2007).
[34] E. L. Wooten, K. M. Kissa, A. Yi-Yan, E. J. Murphy, D. A. Lafaw, P. F. Hallemeier, D. Maack, D. V. Attanasio, D. J. Fritz, G. J. McBrien, and D. E. Bossi, IEEE J. Sel. Top. Quantum Electron. **6**, 69 (2000).